CHEMISTRY OF MATERIALS

ARTICLE

pubs.acs.org/cm

Bulk Synthesis and Structure of a Microcrystalline Allotrope of Germanium (*m-allo*-Ge)

Florian Kiefer,[†] Antti J. Karttunen,[‡] Markus Döblinger,[§] and Thomas F. Fässler*[,†]

[†]Department of Chemistry, Technische Universität München, Lichtenbergstrasse 4, 85747 Garching, Germany

[‡]Department of Chemistry, University of Eastern Finland, P.O. Box 111, FI-80101 Joensuu, Finland

[§]Department of Chemistry, Ludwig-Maximilians-Universität München, Butenandtstrasse 11, 81377 München, Germany

Supporting Information

ABSTRACT: An easy to reproduce and scale-up method for the preparation of a microcrystalline allotrope of germanium is presented. Based on the report of the oxidation of a single crystal of Li_7Ge_{12} the synthesis and structure determination of a powdered sample of Li_7Ge_{12} is investigated. Besides the known oxidation of Li_7Ge_{12} with benzophenone a variety of protic solvents such as alcohols and water were used as oxidants. Electron energy loss spectroscopy (EELS) proves that the reaction products do not contain Li. The structure determination of the powder samples based on selected area electron diffraction (SAED), powder X-ray diffraction, quantum chemical calculations (DFT-B3LYP level of theory), and simulated powder X-ray diffraction diagrams obtained using the DIFFaX and FAULTS software packages show that the microcrystalline powders do not match any of the existing structures of germanium including the rough model of so-called *allo*-Ge. It is shown that the structural motif of layered Ge slabs of the precursor Li_7Ge_{12} that contain five-membered rings is retained in *m*icrocrystalline *allo*-Ge (*m-allo*-Ge). The covalent connectivity between the slabs and the statistic of the layer sequence is determined. According to B3LYP-DFT calculations of a periodic approximate model a direct band gap is expected for *m-allo*-Ge.

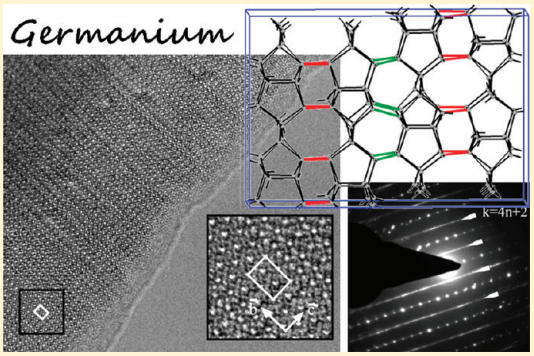

KEYWORDS: allotropy, germanium, modification, stacking fault, structure

INTRODUCTION

The discovery of a class of novel allotropes of carbon, the fullerenes,[1] and the subsequent extension to the material class of carbon nanotubes and fullerides[2] impressively shows that, even though the building blocks and structures are rather simple, the breakthrough has an enormous impact on various fields of research. In this context the straightforward syntheses of hexagonal Ge (4*H*-Ge),[3] the recent discovery of another new crystalline modification of germanium with a clathrate-type porous structure, Ge-cF136,[4] and related mesoporous germanium-based materials[5] are promising candidates to start yet another round of developments in the field of semiconducting materials.[6] Crystalline α-Si and α-Ge are indirect band gap semiconductors and are therefore inefficient light emitters. While all technically important semiconductors such as III−V compounds have a direct band gap and serve as optoelectrical components, the synthesis of elemental direct-band gap semiconductors remains a desirable challenge.[7] Effects on band gaps and absorption coefficients depending on the nature of the material are also observed for amorphous in contrast to crystalline phases of silicon and germanium. For example, the band gap increases, and the absorption coefficient is much higher for amorphous Si.[8] The nature of the Ge band gap for α-Ge to clathrate-type Ge changes likewise.

For the less-studied formation of bulk germanium-based materials it has been shown that binary alkali-metal germanium precursors have a huge synthetic potential.[9] The reaction of compounds containing the $[Ge_9]^{4-}$ anion leads to mesoporous germanium,[5] and even the preservation of the Ge_9 units in germanium materials has been predicted.[10] Another interesting allotrope has been reported which forms through oxidation of Li_7Ge_{12}, and it has been proposed that the topology of the two-dimensional polyanion $^2_\infty[Ge_{12}]^{7-}$ of Li_7Ge_{12} (Figure 1a,b) is retained.[11] The schematic representations in Figure 1c,d show two possibilities of how oxidative coupling can occur under retention of the basic structural units of Li_7Ge_{12} the structure of which has recently been accurately determined.[12] Removal of Li atoms and oxidative coupling of the polyanions lead to the formation of an Li-free compound. A crude structural model of *allo*-Ge has been given based on the unique reaction of a large single crystal of Li_7Ge_{12} with benzophenone/THF and X-ray diffraction of the resulting single crystal with rather poor crystallinity. However, this structure model included disorder on various atom sites, leading to rather unrealistic Ge−Ge distances.

Received: July 11, 2011
Revised: September 15, 2011
Published: September 30, 2011

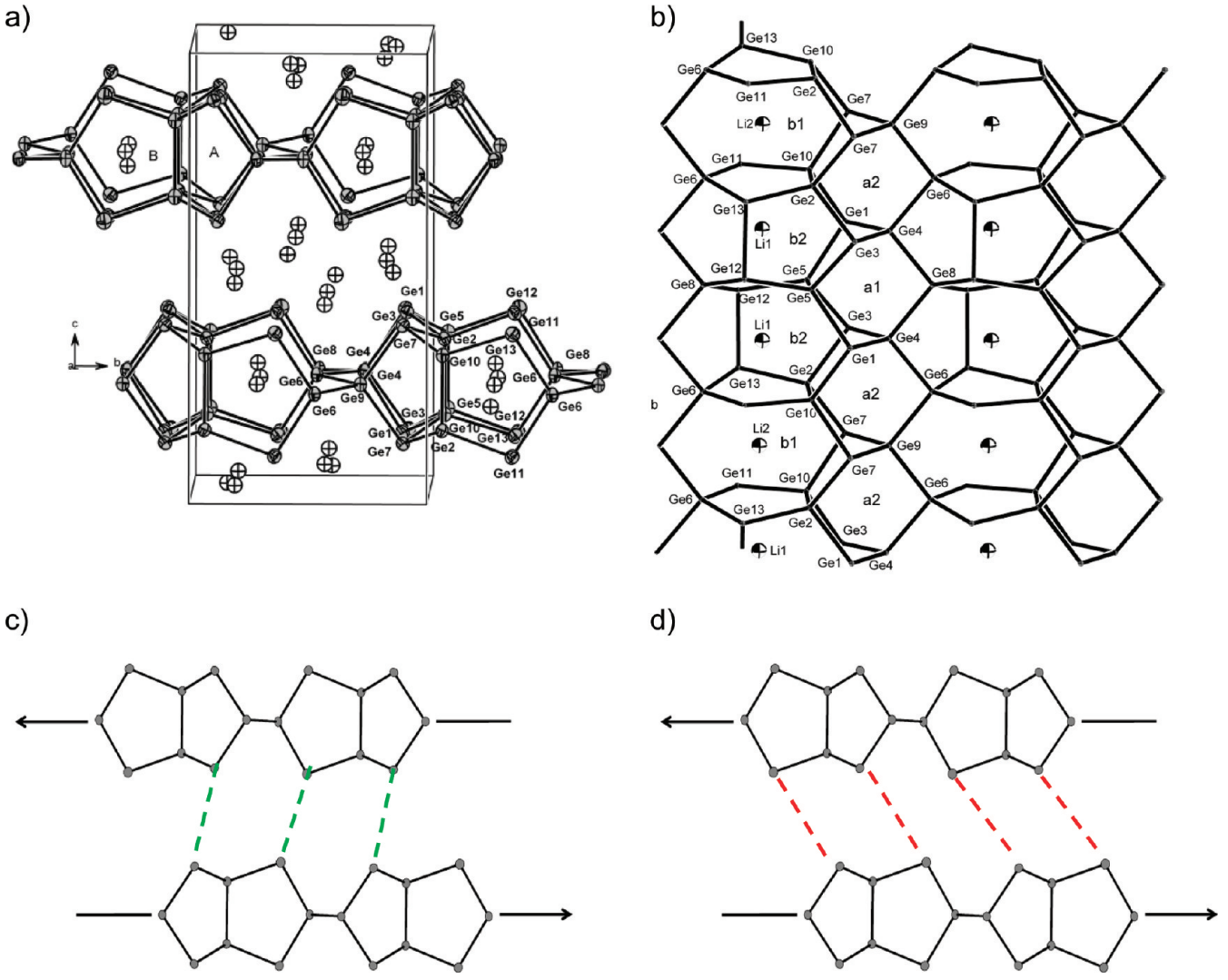

Figure 1. a) Structure of Li_7Ge_{12},[12] b) top view of the polyanions $^2{}_\infty[Ge_{12}]^{7-}$, and c) and d) schematic models of the polyanionic Ge_{12} layers in Li_7Ge_{12} with dashed lines showing possible Ge−Ge connections between the atoms of two adjacent polyanions as expected in *allo*-Ge.

To our knowledge this result has never been reproduced. Further hypothetical structure models of *allo*-Ge are based on theoretical investigations.[13,14] Besides some Raman spectra,[15] a detailed description of *allo*-Ge has not been published thereafter.

We report here about several new and reproducible syntheses for the preparation of *m*icrocrystalline *allo*-Ge (*m-allo*-Ge) starting from Li_7Ge_{12}. Besides the known reaction with benzophenone we used also protic solvents such as H_2O, MeOH, EtOH, and CH_3COOH as oxidants. Since none of the existing models matched our experimental data and since the microcrystalline product differs from the one obtained by reacting a single crystal, we deduced the new structure model for microcrystalline *allo*-Ge based on selected area electron diffraction (SAED), powder X-ray diffraction, quantum chemical calculations (DFT-B3LYP level of theory),[16] and simulated powder X-ray diffraction diagrams obtained using the DIFFaX and FAULTS software packages.

EXPERIMENTAL SECTION

Materials and Reagents. Ge (99.999%) was purchased from Chempur. All other reagents were purchased from Merck and purified using standard laboratory techniques. All manipulations were carried out under inert gas conditions, using standard Schlenk techniques or by working in a glovebox (MBraun, Ar atmosphere, H_2O < 0.1 ppm, O_2 < 0.1 ppm).

Synthesis of Li_7Ge_{12}.[12] The starting materials germanium (0.947 g, 13.0 mmol, granules) and lithium (0.053 g, 7.6 mmol, pieces) were fused by arc melting using a standard welding machine (Edmund Bühler, MAM 1) and a cooled copper reaction plate set in a glovebox. The reaction product is a bright metallic regulus. Besides Li_7Ge_{12} the product might contain also LiGe and α-Ge. The product is ground to a gray powder in an agate mortar, sealed in an Nb or Ta ampule with an arc welder followed by annealing in an oven at 480 °C for seven days. The ampule, which is rapidly cooled in air, now contains single-phase Li_7Ge_{12}.

Synthesis of Microcrystalline *allo*-Ge. The air- and moisture-stable *allo*-Ge was prepared from Li_7Ge_{12} in several reactions using protic solvents or various oxidizing agents. Three mL of the appropriate protic solvents (H_2O, MeOH, EtOH, and CH_3COOH) was added to 1.0 g (1.09 mmol) of single-phase Li_7Ge_{12} in a 20 mL Schlenk tube. In all cases a rapid reaction and the formation of hydrogen was observed, confirmed by a straightforward oxyhydrogen pop test using small amounts of the products. The mixtures were stirred at room temperature for three days, and the solid product was separated by removing liquid components using a cannula. The remaining dark-gray powder was

dx.doi.org/10.1021/cm201976x |*Chem. Mater.* 2011, 23, 4578–4586

washed several times with water. The product was dried under dynamic vacuum for one day. The identity of the products was confirmed by powder X-ray diffraction.

For the reaction with benzophenone, 5 mL (25 mmol) of a 5 molar benzophenone solution in water- and oxygen-free THF was reacted with 4.0 g (4.36 mmol) of Li_7Ge_{12} in a 20 mL Schlenk tube.[11] Three mL of THF was added to this mixture. The reaction solution immediately turned dark blue, indicating the formation of the benzophenone radical according to the equation $Li_7Ge_{12} + 7Ph_2CO \rightarrow 12$*allo*-Ge + 7Li-($Ph_2CO$). The mixture was stirred at room temperature for several days, then all liquid components were removed by a cannula, and the remaining solid was washed with THF until the solution remained colorless. The residue was then washed with toluene, and the remaining volatile products were removed *in vacuo* over one day.

In order to characterize the product, X-ray diffractograms of powdered samples were recorded directly after the reaction. All samples showed identical X-ray patterns.

Powder X-ray Diffraction. Powder X-ray diffractograms were recorded using a Stoe STADI P2 diffractometer (Ge (111) monochromator for Cu$K\alpha_1$ radiation λ = 1.54056 Å) equipped with a linear position sensitive detector PSD with $2\theta_{eff} \sim 40°$. The powder was finely ground in an agate mortar and filled into a glass capillary which was sealed using wax.

Powder X-ray diffraction diagrams were simulated using the DIFFaX and FAULTS software packages.[17,18] DIFFaX exploits the recurring patterns found in randomized stacking sequences to compute the average interference wave function scattered from each layer type occurring in a faulted crystal. FAULTS is based on DIFFaX and allows the refinement of the theoretical structural models with respect to the experimental powder diffraction pattern. Furthermore, DIFFaX can also be used to simulate selected area electron diffraction (SAED) patterns, which can be compared with experimental TEM images. The simulated patterns were generated using monochromatic Cu$K\alpha_1$ radiation (λ = 1.54056 Å) and Pseudo-Voigt instrumental broadening. Background was modeled by linear interpolation. The powder diffraction patterns were simulated with DIFFaX up to $2\theta = 90°$ to confirm agreement with the experiment for high 2θ angles. Due to the significantly higher computational cost of the refinement procedure and the low number of distinctive features for $2\theta > 60°$, the final powder diffraction patterns were refined with FAULTS up to $2\theta = 60°$. The FAULTS and DIFFaX input files are listed in the Supporting Information (Table S1).

Transmission Electron Microscopy (TEM) and Electron Energy Loss Spectroscopy (EELS). The sample was ground in an agate mortar and dispersed in ethyl alcohol suspension. A small amount of the suspension was dispersed on a copper grid coated with a holey carbon film. The grids were mounted on a double tilt holder with a maximum tilt angle of 30° and subsequently transferred into the microscope. Electron microscopy was carried out on a FEI Titan 80-300 instrument equipped with a field emission gun operating at 300 kV. TEM images and electron diffraction patterns were recorded on a Gatan UltraScan 1000 P CCD camera. EELS was performed with a Gatan Tridiem 863 P spectrometer.

Computational Details. The germanium structures were investigated using the B3LYP hybrid density functional and localized atomic basis sets composed of Gaussian-type functions. All calculations were performed using the CRYSTAL06 and CRYSTAL09 software packages.[19] In periodic calculations, the choice of the Gaussian-type localized atomic basis set requires careful consideration. Basis sets originally developed for molecular calculations contain diffuse basis functions to model the tails of wave functions, but in periodic calculations, where the whole space is filled with basis functions, such diffuse functions are usually unnecessary and lead into numerical difficulties and/or severe degradation of performance.[20] A split-valence-quality basis set, originally developed by Ruiz et al.,[21] and later reoptimized for elemental germanium,[3] was applied in all calculations. The results obtained for germanium modifications at the present B3LYP/SVP level of theory have previously been confirmed to be in agreement with results obtained using the PBE0 hybrid functional and the SVP basis set.[10] In structural optimizations, both the cell parameters and the atomic positions of the studied sample were allowed to relax within the constraints imposed by the space group symmetry. The shrinking factors (SHRINK) used for generating a Monkhorst-Pack-type grid of *k*-points in reciprocal space were as follows: Chadi models: 8; Conesa models: 4; Nesper model; and the GA+GB model (128 atoms/cell): 2. For the evaluation of the Coulomb and exchange integrals (TOLINTEG), very tight tolerance factors of 10, 10, 10, 10, and 20 were used. Default optimization convergence thresholds and extra large integration grid (XLGRID) for the density-functional part were applied in the calculations. Vibrational frequencies were obtained by using the computational scheme implemented in CRYSTAL.[19]

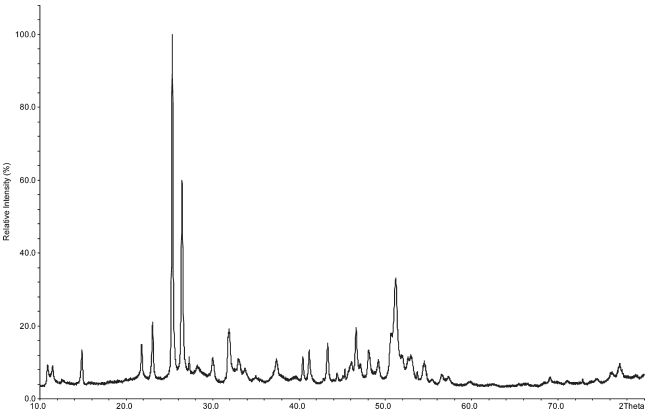

Figure 2. Experimental powder X-ray diffraction diagram of *m-allo*-Ge.

RESULTS

Synthesis of *m-allo*-Ge. *Microcrystalline allo*-Ge was synthesized from single-phase Li_7Ge_{12} using protic solvents such as water and alcohols as well as benzophenone (in THF) as oxidizing agent. Li_7Ge_{12} was stirred with the appropriate solvent for several days under the exclusion of air. After removal of all volatile components and washing, the dried products showed identical characteristic powder X-ray diffractograms (Figure 2). The absence of the Li K edge in electron energy loss spectra (EELS) proves that the reaction products do not contain Li within the limits of detection (Supporting Information Figure S1).

Structure Determination of *m-allo*-Ge. The powder diffraction pattern was indexed by an orthorhombic cell with a = 7.9, b = 16.3, and c = 11.9 Å (Figure 3a,b) determined by electron diffraction. The setting of the orthorhombic cell of *m-allo*-Ge was chosen with respect to corresponding orientations of the cell axes of Li_7Ge_{12}. Assuming a simple removal of the Li atoms from Li_7Ge_{12}, the Li interlayers shown in Figure 1 collapse, and the structure contracts along c from 15.35 Å in Li_7Ge_{12} to 11.9 Å in *m-allo*-Ge. In all electron diffraction patterns observed, reflections appearing on lines with $h = 2n+1$ are very weak (Figure 3a). On the remaining reciprocal lines ($h = 2n$) in $hk0$ patterns, we observed that the reflections with $k = 2n+1$ are either very weak or completely absent. These two observations suggest that *m-allo*-Ge can be described with respect to a basic structure with the lattice parameters a = 3.9 and b = 8.1 Å.

dx.doi.org/10.1021/cm201976x |*Chem. Mater.* 2011, 23, 4578–4586

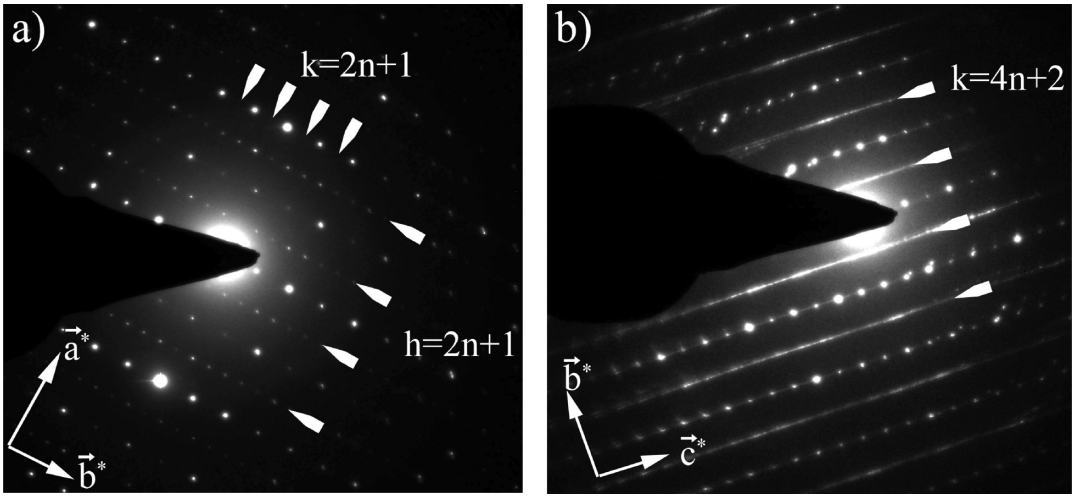

Figure 3. Selected area electron diffraction patterns of *m-allo*-Ge showing the reciprocal *hk*0 layer (a) and the 0*kl* layer (b). In (a), the weak reflections on lines with $h = 2n+1$ and the absence of reflections with $k = 2n+1$ on the remaining lines indicate a basic structure, as described in the text. The 0*kl* plane shown in (b) exhibits diffuse streaks located on lines along c^* fulfilling $k = 4n+2$ and the reflections with $k = 2n+1$ are absent. The reciprocal space vectors shown in the micrographs are not true to scale.

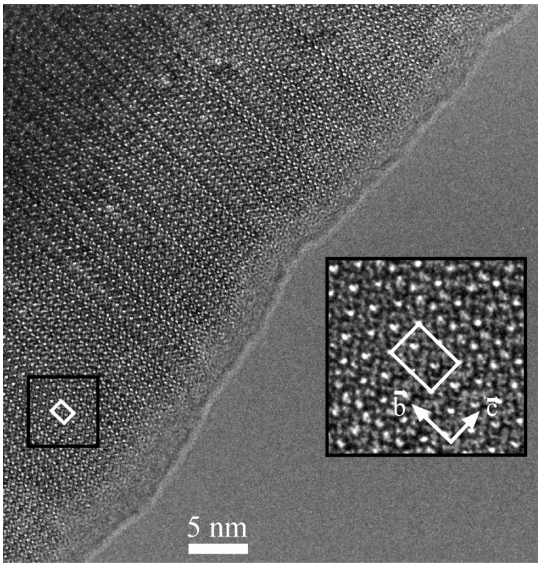

Figure 4. HRTEM image of *m-allo*-Ge recorded along [100]. While being perfectly periodic along *b*, the image reveals considerable disorder along *c*. The area outlined by a black box is enlarged on the right side of the figure. The white box indicates the projected unit cell.

Further, 0*kl* patterns, as represented in Figure 3b, exhibit lines of diffuse streaks for $k = 4n+2$, and reflections with $k = 2n+1$ are absent. This indicates a glide plane perpendicular to *a* in *b* direction and that the periodicity of 8.1 Å along *b* is only weakly correlated along *c*. This can also be seen in a representative HRTEM image recorded along [100] shown in Figure 4.[22] Since the structure appears well ordered along *a* and *b* but disordered along *c*, this model suggests that the polyhedron type found in the two-dimensional slabs of Li_7Ge_{12} and thus the order in the *ab* plane of *m-allo*-Ge as shown in Figure 1 are retained upon oxidation of Li_7Ge_{12}. In contrast, the disorder along *c* in *m-allo*-Ge shows a nonregular connection between the Ge atom slabs.

Various Structural Models of *allo*-Ge. We applied quantum chemical methods to investigate the various structural models for *allo*-Ge. The 16-atom model previously suggested by Chadi,[14] which is directly related to the layered structure of Li_7Ge_{12}, is denoted here as model **1** (Figure 5a). As pointed out in Figure 1c, the model can be created by shifting two adjacent polyanion layers in Li_7Ge_{12} against each other in the *b* direction. The cell parameters of the basic structure (a = 3.9 and b = 8.1 Å) are in good agreement with this model, and the substructure of Ge from Li_7Ge_{12} is also mostly preserved. However, the simulated powder X-ray and electron diffraction patterns on the basis of the structure model by Chadi agree very poorly with the observed diffraction patterns (Supporting Information Figure S2). Conesa has performed a systematic investigation of different *allo*-Ge models by studying the different ways of interconnecting the Ge layers after the removal of Li atoms from the Li_7Ge_{12} structure.[13] He investigated more than 40 structural models derived from Li_7Ge_{12}, classifying the different structure types as GA, GB, GC, or GD depending on the interlayer connectivity and orientation of the Ge layers. Two representative structural models of the GA- and GB-type families are shown in Figure 5b,c (models **2** and **3**). In the GA and GB structures of Conesa, the Ge layers are alternating in a similar way as in the parent Li_7Ge_{12}, while in the GC and GD structure types (not shown here), all layers are oriented in the same direction, contradicting the Li_7Ge_{12} structure. We have also included the original 128 atom structural model of Nesper et al. (model **4** in Figure 2d).[11] We retained the original lattice constants of Nesper et al. but optimized the atomic positions to obtain a germanium framework with realistic bond lengths, since retaining the original atomic positions resulted in several Ge−Ge bonds that are shorter than 2 Å. Furthermore, *allo*-Ge was originally noted to display considerable stacking disorder, which is not accounted for in the model **4**. As discussed by Conesa, all Ge layers in the Nesper model are oriented in the same direction, different from the Li_7Ge_{12} structure with alternating layer orientations.[13]

We calculated the relative energies of the studied Chadi, Conesa, and Nesper models (Figure 6) and compared them to

dx.doi.org/10.1021/cm201976x |*Chem. Mater.* 2011, 23, 4578–4586

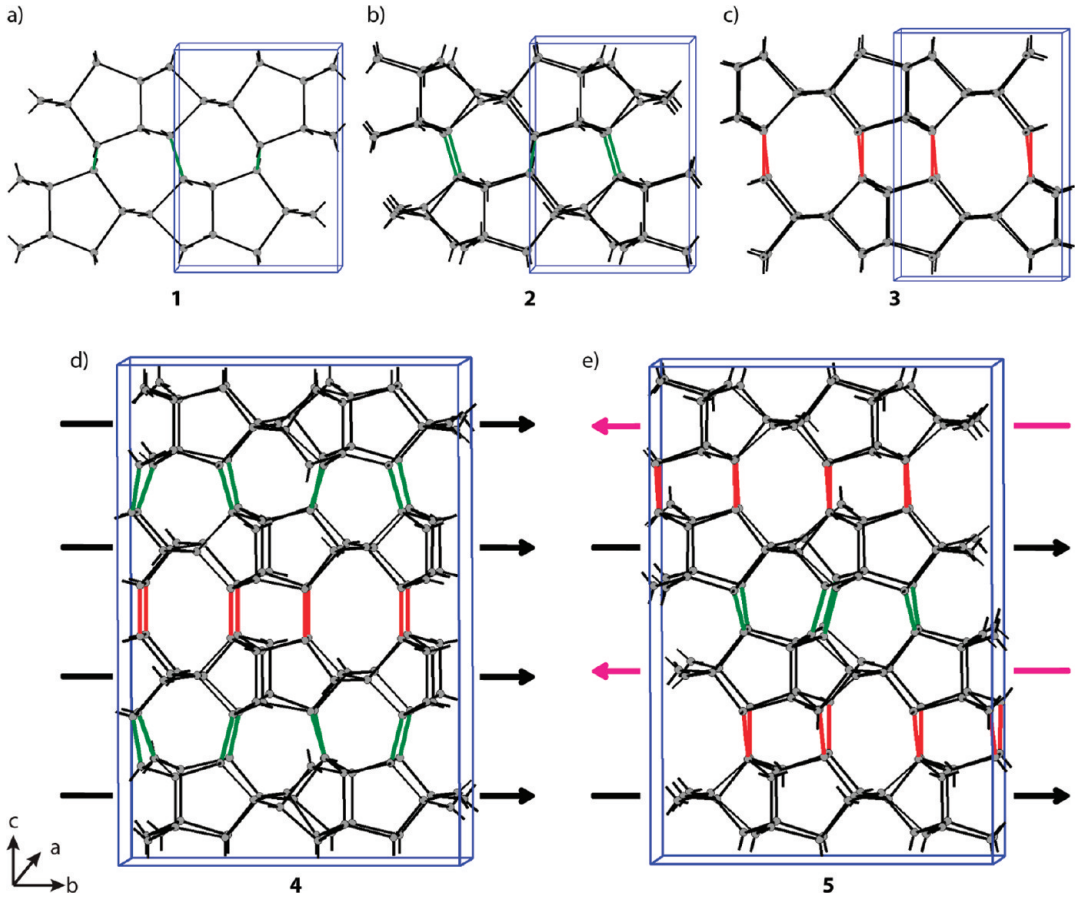

Figure 5. Schematic illustrations of the unit cells of various structural models for *allo*-Ge (the unit cell edges are drawn in blue). a) Chadi's model with 16 Ge atoms per unit cell containing 7-membered rings (highlighted with green), b) Conesa's model GA with 32 atoms per unit cell containing 7-membered rings, c) Conesa's model GB with 32 atoms per unit cell containing 6- and 8-membered rings (highlighted with red), d) Nesper's model with 128 atoms per unit cell, e) new merged model based on model GA and GB with alternating layer direction (128 atoms/unit cell). The arrows in d) and e) denote the orientation of the two-dimensional layers of the Ge atoms of the polyanion in Li_7Ge_{12} as depicted in Figure 1.

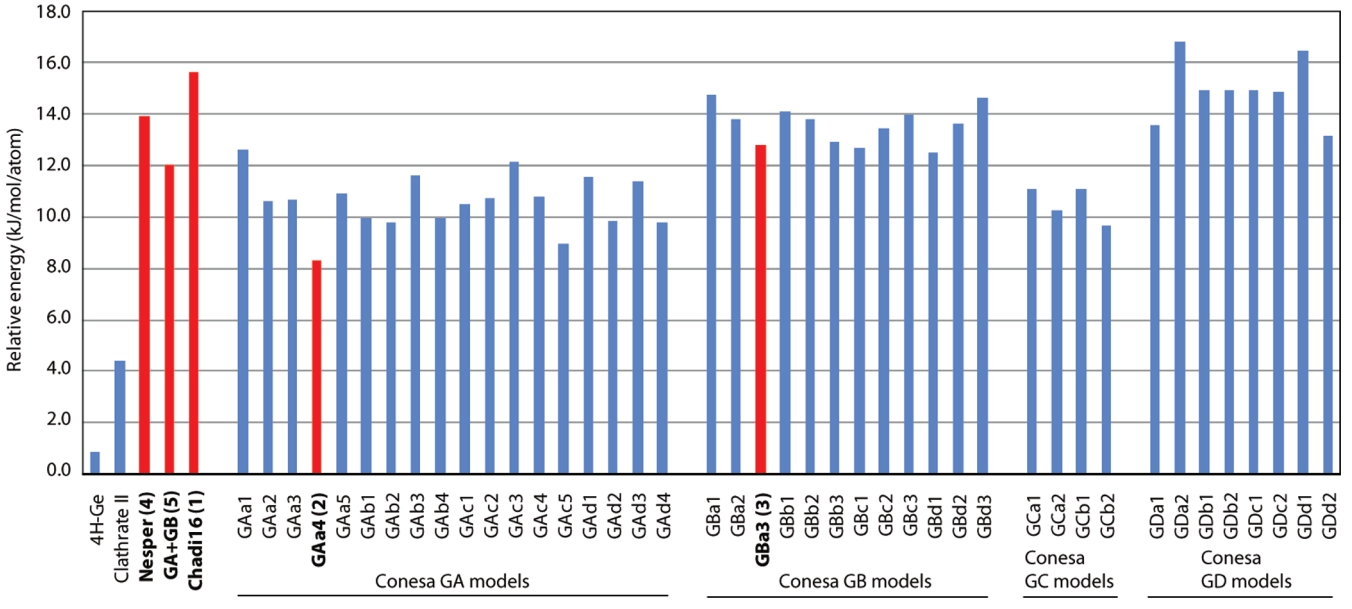

Figure 6. The relative energies of the various structural models of *allo*-Ge. The energies in kJ/mol/atom are given relative to α-Ge. Two existing crystalline modifications of germanium are shown for comparison (4H−Ge[3] and Clathrate-II[4]).

dx.doi.org/10.1021/cm201976x |*Chem. Mater.* 2011, 23, 4578–4586

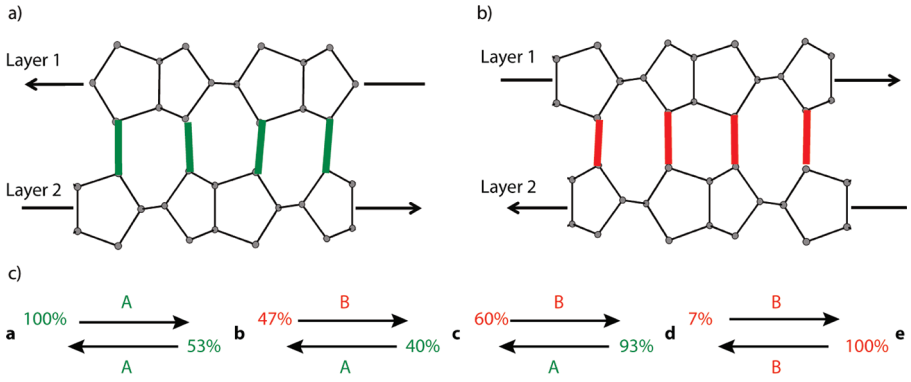

Figure 7. The structural model **6** of *allo*-Ge with stacking faults based of a statistical sequence of a) interlayer connection **A** including 7-membered rings and b) interlayer connection **B** including 6- and 8-membered rings. c) Transition probability of the occurrence of the interlayer connection type **A** and **B**. Layers (a, c, e) and (b, d) in Figure 7c correspond to the layer types 1 and 2 in Figure 7a-b, respectively. See text for more details.

4*H*-Ge and Ge-cF136. In agreement with the results of Conesa, the GAa4 model (**2**) is energetically the most favorable one, being 8.3 kJ/mol/atom less stable than α-Ge. For comparison, the recently investigated hexagonal 4*H*-Ge and the clathrate-type Ge-cF136 are 0.9 kJ/mol/atom and 4.4 kJ/mol less stable than α-Ge, respectively.[3,4] The GB models of Conesa are more strained than the GA models. The Nesper model (**4**) is energetically close to the Conesa GB models, while the Chadi-16 model (**1**) is one of the most strained ones. All studied Ge phases are covalently bonded, and the stability order of the phases depends on their structural characteristics with respect to the most stable phase, α-Ge (Ge−Ge bond length 2.45 Å, all bond angles 109.5°). Deviations from the perfect tetrahedral arrangement will induce structural strain. For example, in the experimentally determined structure of the porous Clathrate-II structure, the bond lengths vary between 2.43−2.51 Å and the bond angles are 106.0−120.0°. In the more strained *allo*-Ge models, the deviations from α-Ge are considerably larger, in particular for the bond angles. In the most favorable GAa4 model (**2**), the bond lengths are 2.40−2.57 Å, and the bond angles are 92.7−126.2° (the lattice parameters of the optimized structures were scaled by 0.98 to enable direct comparisons with the experiment). In the case of the more strained GBa3 model, the bond lengths are fairly similar to those in GAa4 (2.38−2.56 Å), but the bond angles deviate even more from the ones in α-Ge (92.1−135.3°). In the Nesper model (**4**), the bond lengths are also similar to those in GAa4 (2.38−2.54 Å), but the largest bond angles are increased even further (89.9−144.9°). Finally, in the least favorable Chadi-16 model with the smallest unit cell among the studied models, the bond lengths vary between 2.39−2.56 Å, and the structure possesses some very small and strained bond angles (89.7−128.3°). All studied *allo*-Ge structures are semiconducting according to our DFT-B3LYP calculations, and the energetically most favorable GAa4 structure shows a direct band gap of 1.26 eV (Figure S3, Supporting Information).

The simulated powder diffraction patterns of the structural models **1**-**4** are very different from the experimental ones (Supporting Information Figure S2). The models **2** and **4** show a large portion of the features visible in the experimental spectrum, but the overall match is rather poor. Our first attempt to improve the previous structural models was to introduce a simple modification based on the results of Conesa. The model **5**, resulting from the combination of the GA and GB structural motifs, is closely related to the Nesper model (Figure 5), but the Ge layers show an alternating orientation in agreement with the Li_7Ge_{12} structure. The lattice constants and atomic positions of the model were fully optimized with DFT. The relative energy of the structure **5** is 12.0 kJ/mol/atom, which is an intermediate of the GA and GB models, as can be expected from the structural characteristics. However, the match between the simulated powder diffraction pattern and the experimental one was still not very good (Supporting Information Figure S2).

The rather poor correlation between the simulated powder diffraction patterns of the structural models **1**−**5** and experimental ones suggests that a more complex structural model is required to reproduce the experimental powder diffraction pattern of *m-allo*-Ge. The synthesis of *m-allo*-Ge from the Li_7Ge_{12} precursor proceeds through a rapid topotactical reaction, resulting in imperfect stacking and stacking faults in the structure. The presence of stacking faults is confirmed by the TEM measurements (Figures 3b and 4). Therefore, we created a structural model with stacking faults and simulated the powder diffraction patterns with the DIFFaX and FAULTS software packages.[17,18]

Based on the results for the more simple models **1**−**5**, we created a new structural model **6** (Figure 7). As a starting point for this model we used the GAa4 model of Conesa that is the energetically most favorable ordered model. In model **6**, the energetically most favorable stacking mode with consecutive **A** interlayers is considered as normal stacking, while **B**-type interlayers are considered as stacking faults. To reproduce the features of the experimental powder diffraction pattern, the stacking scheme shown in Figure 7c had to be applied for the two layer types present in Li_7Ge_{12}. In this scheme, the total probabilities of **A**- and **B**-type interlayer contacts are 60% and 40%, respectively, also in agreement with the energetically favorable **A**-type stacking. Further, more than two consecutive **B**-type connections (for example, b → c → d → e) are very improbable in this model. Schemes with simpler stacking schemes failed to reproduce the experimental powder X-ray diffraction pattern. A preliminary version of the structural model **6** was first created using the DIFFaX software, after which the model was refined with respect to the experimental data using the FAULTS software. The *a* and *b* cell parameters of model **6** are 7.79 and 8.15 Å, respectively. Experimental values from TEM are $a = 7.9$, $b = 16.3$ Å. The height of one **A** or **B** interlayer (that is, two Ge-layers) in the *c* direction is 11.7 Å, which is in rather good agreement with the experimentally

dx.doi.org/10.1021/cm201976x |*Chem. Mater.* 2011, 23, 4578–4586

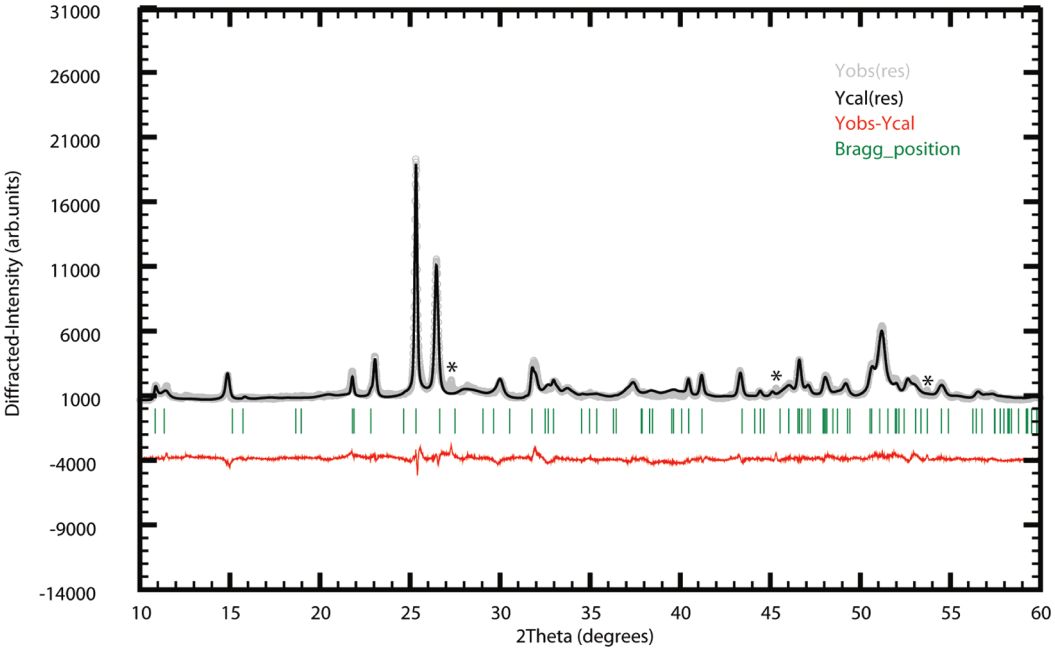

Figure 8. Powder X-ray diffractogram of the *m-allo*-Ge. Experimental data are shown as a gray line; reflections based on structural model **6** with stacking faults along the *c* axis are simulated with the FAULTS software and shown as a black line. The difference diagram is shown in red. Reflections denoted with (*) originate from α-Ge.

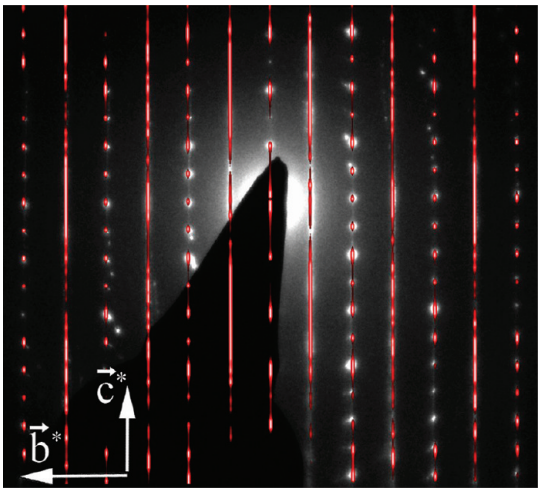

Figure 9. Simulated electron diffraction pattern for the *allo*-Ge model **6** (red) superimposed on an experimental electron diffraction pattern of *m-allo*-Ge (reciprocal *0kl* layer, cf. Figure 3b).

observed $c = 11.9$ Å. The values for *a* and *c* fit very well with our experimental observations by TEM. The doubled lattice constant experimentally determined for *b* (16.3 Å) is the result of a weak superstructure, as indicated by the weak reflections with indices $k = 2n+1$ in Figure 3a. These superstructure reflections are not visible in the powder diffraction pattern. The exact relative energy or the band gap of model **6** cannot be obtained from theory, as the statistical part of the model cannot be described by quantum chemical calculations which always require an ordered model. However, similar to the ordered structural model **5**, the relative energy of model **6** is expected to be an intermediate between the GA and GB parent structures.

The simulated powder diffraction pattern resulting from the structural model **6** is shown in Figure 8. All reflections of the experimental data occur in the simulated X-ray diffraction diagram, and the intensities agree well. The match between the simulated and the experimental pattern is noticeably better in comparison to the patterns of the ordered models (Supporting Information Figure S2). The sample contains small amounts of α-Ge (sharp peaks at 27.3°, 45.3°, and 53.7°). The performance of the structural model **6** in terms of the profile *R*-factor R_p (8.0%) is comparable to similar stacking models in the literature.[23] The simulated SADP image for the structural model **6**, together with the experimental TEM image, is shown in Figure 9.

DISCUSSION

The allotropes of germanium and the germanium-based porous materials play a crucial role in understanding intrinsic semiconductors. Recently the clathrate-type germanium allotrope was structurally characterized and found to be a semiconductor with a direct band gap, whereas porous materials show various types of band gaps.

Up to now A_4Ge_9 phases (A = alkali metal), which contain discrete clusters, were mainly used for the formation of Ge-based materials.[4,9] The wide variety of reactions presented here shows that Li_7Ge_{12} with a layered structure is an alternatively good precursor for the soft formation of germanium-based materials at room temperature. The reaction strategy to remove alkali metals from layered Zintl phases has now been successfully demonstrated for Li_7Ge_{12} and might also apply for other layered compounds. In our case, covalent Ge−Ge bonds are formed, and simultaneous deintercalation and oxidative bond formation at low temperatures lead to novel metastable materials which are otherwise elusive. The scattering experiments of *m-allo*-Ge reveal

dx.doi.org/10.1021/cm201976x |*Chem. Mater.* 2011, 23, 4578–4586

the long-range order in this material and show that the Ge network of the binary phase Li_7Ge_{12} is mainly preserved, even though a certain degree of freedom in connecting the Ge layers is possible.

The high reactivity of *allo*-Ge is indicated by the structural transformation of *allo*-Ge to 4*H*-Ge, since five-membered rings in *allo*-Ge transform to six-membered rings in 4*H*-Ge. This transformation already starts at 140 °C. Recently, we published a detailed study of the transformation of *allo*-Ge to 4H Ge.[3] Interestingly, even though the transition occurs at a very low temperature as compared to the melting point of α-Ge, a microcrystalline and not an amorphous powder is obtained. Preliminary reactions of *m-allo*-Ge with the alkali metals Rb and Cs show that RbGe and CsGe are already formed below 100 °C and not at several hundred degrees Celsius when starting from α-Ge.[24]

CONCLUSION

Allotropes of elements count in many respects to the simplest systems and at the same time — due to their structural simplicity — they hold a huge potential in understanding the structure—property relationship of materials. Especially the allotropes of the elements of the carbon group have the outstanding property to switch from insulators to conductors (carbon) or from semimetals to metals (tin) by changing their modification. Therefore the synthesis of element allotropes is a high challenge. In this article we present the synthesis of a crystalline Ge allotrope whose structure is predetermined by the precursor Li_7Ge_{12}. Most astonishing is the fact that through deintercalation the structure of the precursor that contains five-membered Ge polygons is retained and that the topotactic formation through oxidation of two-dimensional Ge slabs of the precursors can be scrutinized in the product *m-allo*-Ge. Due to rather small impurities of α-Ge, band gap measurements of microcrystalline *m-allo*-Ge are not yet significant. From theoretical calculations of ordered variants a direct band gap is expected. The microcrystalline metastable *m-allo*-Ge is transformed through thermal activation in a first step to hexagonal germanium and finally to the most stable modification cubic germanium. The synthesis by means of an oxidative delithiation of a binary Li—Ge phase offers a valuable method which should apply to other Li-containing phases and presents an interesting alternative to the recently reported oxidation of alkali metal germanides in ionic liquids. In contrast to other routes, the method reported here offers the synthesis of bulk materials in quantities of several grams.

ASSOCIATED CONTENT

Supporting Information. EEL spectrum of *allo*-Ge, simulated powder diffraction patterns for the structural models **1**—**5**, and FAULTS and DIFFaX input files for the structural model **6** as well as the band structure diagram of the ordered GAa4 structure. This material is available free of charge via the Internet at http://pubs.acs.org.

AUTHOR INFORMATION

Corresponding Author

*Fax: +49-89-28913186. E-mail: Thomas.faessler@lrz.tum.de.

ACKNOWLEDGMENT

F.K. thanks the Foundation of the German Economy for financial support. A.J.K. gratefully acknowledges financial support from the Finnish Funding Agency for Technology and Innovation, European Union/European Regional Development Fund (grant 70026/08), and the Academy of Finland (grant 138560/2010). We thank Dr. Montse Casas Cabanas (Laboratoire de Crystallographie et Sciences de Matériaux, Caen, France) for providing us with a copy of the FAULTS software. We like to thank Dr. A. Schier for the revision of the manuscript.

REFERENCES

(1) Kroto, H. W.; Heath, J. R.; O'Brien, S. C.; Curl, R. F.; Smalley, R. E. *Nature* **1985**, *318*, 162–163. Krätschmer, W.; Lamb, L. D.; Fostiropoulos, K.; Huffman, D. R. *Nature* **1990**, *347*, 354–358.

(2) The carbon nanotubes which had recently been discovered are not crystalline.Iijima, S. *Nature* **1991**, *354*, 56–58.Dresselhaus, M. S.; Dresselhaus, G.; Eklund, P. C. *Science of Fullerenes and Carbon Nanotubes*; Academic Press: New York, 1996. Hebard, A. F.; Rosseinsky, M. J.; Haddon, R. C.; Murphy, D. W.; Glarum, S. H.; Palstra, T. T. M.; Ramirez, A. P.; Kortan, A. R. *Nature* **1991**, *350*, 600–601. Reed, C. A.; Bolskar, R. D. *Chem. Rev.* **2000**, *100*, 1075–1120.

(3) Kiefer, F.; Hlukhyy, V.; Karttunen, A. J.; Fässler, T. F.; Gold, C.; Scheid, E.-W.; Scherer, W.; Nylén, J.; Häussermann, U. *J. Mater. Chem.* **2010**, *20*, 1780–1786.

(4) Guloy, A. M.; Ramlau, R.; Tang, Z.; Schnelle, W.; Baitinger, M.; Grin, Y. *Nature* **2006**, *443*, 320–323.

(5) (a) Armatas, G. S.; Kanatzidis, M. G. *Nature* **2006**, *441*, 1122–1125. (b) Sun, D.; Riley, A. E.; Cadby, A. J.; Richman, E. K.; Korlann, S. D.; Tolbert, S. H. *Nature* **2006**, *441*, 1126–1130. (c) Stein, A. *Nature* **2006**, *441*, 1055–1056. (e) Armatas, G. S.; Kanatzidis, M. G. *Science* **2006**, *313*, 817–820. (d) Armatas, G. S.; Kanatzidis, M. G. *Adv. Mater.* **2008**, *20*, 546–550.

(6) Fässler, T. F. *Angew. Chem., Int. Ed.* **2007**, *46*, 2572–2575.

(7) For a design of direct band gap semiconductors, see: Zhang, P.; Crespi, V. H.; Chang, E.; Louie, S. G.; Cohen, M. L. *Nature* **2001**, *409*, 69–71.

(8) (a) Kubinyi, M.; Grofcsik, A.; Jeremy Jones, W. *J. Mol. Stuct.* **1997**, *408*, 121–124. (b) Kux, A.; Ben Chorin, M. *Phys. Rev. B* **1995**, *51*, 17535–17541. (c) Clark, A. H. *Phys. Rev.* **1967**, *154*, 750–757. (d) Tauc, J.; Grigorovici, R.; Vancu, A. *Phys. Status Solidi* **1966**, *15*, 627–637.

(9) (a) The reaction of $CaGe_2$ with HCl leads to polygermyne (ref 9b.). The reaction of M_4Si_4 (M = Na, K) containing $[Si_4]^{4-}$ with HCl or H_2O leads to the formation of clathrates M_8Si_{46} (ref 9c.). (b) Vogg, G.; Brandt, M.; Stutzmann, M. *Adv. Mater.* **2000**, *12*, 1278–1281. (c) Böhme, B.; Guloy, A.; Tang, Z.; Schnelle, W.; Burkhardt, U.; Baitinger, M.; Grin, Y. *J. Am. Chem. Soc.* **2007**, *129*, 5348–5349.

(10) Karttunen, A. J.; Fässler, T. F.; Linnolahti, M.; Pakkanen, T. A. *Chem. Phys. Chem.* **2010**, *11*, 1944–1950.

(11) (a) Grüttner, A.; Nesper, R.; von Schnering, H.-G. *Angew. Chem., Int. Ed.* **1982**, *21*, 912–913.(b) A. Grüttner, *Dissertation*, University of Stuttgart, 1982. (c) Related results on *allo*-Si are found in the following: von Schnering, H.-G.; Schwartz, M.; Nesper, R. *J. Less-Common Met.* **1988**, *137*, 297-310.

(12) Kiefer, F.; Fässler, T. F. *Solid State Sci.* **2011**, *13*, 636–640.

(13) Conesa, J. C. *J. Phys. Chem. B* **2002**, *106*, 3402–3409.

(14) Chadi, D. *J. Phys. Rev. B* **1985**, *32*, 6485–6489.

(15) Lopez-Cruz, E.; Cardona, M. *Solid State Commun.* **1983**, *45*, 787–789.

(16) (a) Becke, A. D. *J. Chem. Phys.* **1993**, *98*, 5648–5652. (b) Stephens, P. J.; Devlin, F. J.; Chabalowski, C. F.; Frisch, M. J. *J. Phys. Chem.* **1994**, *98*, 11623–11627.

(17) (a) Treacy, M. M. J.; Newsam, J. M.; Deem, M. W. *Proc. R. Soc. London, Ser. A* **1991**, *A433*, 499–520.(b) http://www.public.asu.edu/~mtreacy/DIFFaX.html (accessed September 28, 2011).

(18) Casas-Cabanas, M.; Rodriguez-Carvajal, J.; Palacin, M. R. *Z. Kristallogr.* **2006**, *23*, 243–248.

(19) (a) Dovesi, R.; Saunders, V. R.; Roetti, C.; Orlando, R.; Zicovich-Wilson, C. M.; Pascale, F.; Civalleri, B.; Doll, K.; Harrison,

N. M.; Bush, I. J.; D'Arco, Ph.; Llunell, M. *CRYSTAL06 User's Manual*; University of Torino, Torino, 2006. (b) Dovesi, R.; Saunders, V. R.; Roetti, R.; Orlando, R.; Zicovich-Wilson, C. M.; Pascale, F.; Civalleri, B.; Doll, K.; Harrison, N. M.; Bush, I. J.; D'Arco, P.; Llunell, M. *CRYSTAL09 User's Manual*; University of Torino: Torino, 2009. (c) Dovesi, R.; Orlando, R.; Civalleri, B.; Roetti, R.; Saunders, V. R.; Zicovich-Wilson, C. M. *Z. Kristallogr.* **2005**, *220*, 571–573.

(20) Kudin, K.; Scuseria, G. E. *Phys. Rev. B* **2000**, *61*, 16440–16453.

(21) (a) Ruiz, E.; Llunell, M.; Alemany, P. *J. Solid State Chem.* **2003**, *176*, 400–411.(b) CRYSTAL basis set library at http://www.crystal.unito.it (accessed September 28, 2011).

(22) The largest area observed by HRTEM with an ordered structure along c extends over 3.6 nm (3 periods).

(23) (a) Casas-Cabanas, M.; Rodriguez-Carvajal, J.; Palacin, M. R. *Powder Diffr.* **2005**, *20*, 334–344. (b) Casas-Cabanas, M.; Rodriguez-Carvajal, J.; Canales-Vazquez, J.; Laligant, Y.; Lacorre, P.; Palacin, M. R. *J. Power Sources* **2007**, *174*, 414–420.

(24) Busmann, E. *Z. Anorg. Allg. Chem.* **1961**, *313*, 90.